Shaping Giant Membrane Vesicles in 3D-Printed Protein Hydrogel Cages

*Haiyang Jia, Thomas Litschel, Michael Heymann, Hiromune Eto, Henri G. Franquelim, and Petra Schwille**

Giant unilamellar phospholipid vesicles are attractive starting points for constructing minimal living cells from the bottom-up. Their membranes are compatible with many physiologically functional modules and act as selective barriers, while retaining a high morphological flexibility. However, their spherical shape renders them rather inappropriate to study phenomena that are based on distinct cell shape and polarity, such as cell division. Here, a microscale device based on 3D printed protein hydrogel is introduced to induce pH-stimulated reversible shape changes in trapped vesicles without compromising their free-standing membranes. Deformations of spheres to at least twice their aspect ratio, but also toward unusual quadratic or triangular shapes can be accomplished. Mechanical force induced by the cages to phase-separated membrane vesicles can lead to spontaneous shape deformations, from the recurrent formation of dumbbells with curved necks between domains to full budding of membrane domains as separate vesicles. Moreover, shape-tunable vesicles are particularly desirable when reconstituting geometry-sensitive protein networks, such as reaction-diffusion systems. In particular, vesicle shape changes allow to switch between different modes of self-organized protein oscillations within, and thus, to influence reaction networks directly by external mechanical cues.

1. Introduction

Bottom-up reconstitution of well-characterized functional biomaterials, such as molecular entities, parts, and modules, with the final goal of constructing a synthetic cell, is a fascinating variant of Synthetic Biology.[1] Although this goal may not easily be within reach in the next years and potentially decades, cell-free reconstitution of fundamental biological functions has interesting implications for research on the origin of life[2] on one hand, and may open up new potential applications from medicine to technology on the other hand.[3] In order to accomplish large-scale biomimetic behavior and realize the vision of a fully functional synthetic cell, a large number of cutting-edge tools or technologies inspired by nanotechnology and material science have been developed and favorably employed.[4] With regard to providing a maximally biocompatible and biomimetic compartment as a first step toward a cell-like reaction space, giant unilamellar vesicles (GUVs) composed of phospholipids have in the past years gained great attention.[5] GUV membranes mimic cellular membranes in many relevant aspects, their lipid composition can be tuned over a wide range,[6] they can be supported by a minimal cortex,[7] and even large transmembrane proteins can be reconstituted into them.[8] However, many advanced protein functionalities like cell division, differentiation, migration, and signaling require the establishment of spatial anisotropy, or in other words, polarization,[9] which is hard to realize in spherical vesicles. In particular, reconstituted bacterial cell division machineries that are supposed to ultimately induce controlled vesicle splitting have been shown to require elongated geometries with distinct symmetry axes.[10]

Thus, developing ways for a controlled deformation of GUVs into desired shapes, resulting in an anisotropic membrane or a polar physical microenvironment, will greatly improve our toolbox for the bottom-up reconstitution of biological functionality toward a synthetic cell. So far, several methods to template membrane vesicles and induce anisotropic structure in vitro have been developed, like microfluidics,[11] micropipette aspiration, optical tweezers, and dielectrophoretic field cages.[12] However, most of them require sophisticated technology or are unable to dynamically control the membrane geometry in a well-defined, i.e., precise and programmable, manner. On the other hand, cell biology-derived tools like 2D micropatterning,[13] hydrogels in 3D-printed microchannels,[14] and 3D soft lithography of hydrogel[15] have been successfully applied to control interfacial geometry in order to define the extracellular environment. Since the development of 3D printing technology, rationally designed 3D objects can be produced from various materials on different scales. In this context, stimuli-responsive hydrogels, which can cycle between expanded and condensed states in response to environmental triggers (e.g., pH, ionic strength), could constitute an attractive material for 3D or 4D Printing.[16] In fact, pH-responsive Bovine serum albumin (BSA) hydrogels are already widely used to fabricate 3D
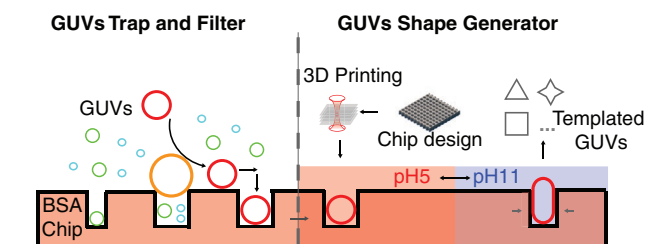
Dr. H. Jia, T. Litschel, Dr. M. Heymann, H. Eto, Dr. H. G. Franquelim, Prof. P. Schwille
Max Planck Institute of Biochemistry
Am Klopferspitz 18, D-82152 Martinsried, Germany
E-mail: schwille@biochem.mpg.de

**ADVANCED
SCIENCE NEWS**

www.advancedsciencenews.com

NANO · MICRO

small

www.small-journal.com

Figure 1. Concept of 3D-printed protein hydrogel trapping and templating giant vesicles (GUVs).

tissue scaffolds[17] and generating smart 4D stimuli-responsive microactuators.[16,18]

Here, we varied and expanded this technology toward the goal of selectively trapping GUVs within a customized 3D printed BSA hydrogel chip, and dynamically inducing structural anisotropy by applying external pH stimuli to the gel. The basic working principle is illustrated in **Figure 1**. 3D printed protein hydrogel can be designed as microchambers in appropriate sizes for capturing GUVs. The variable protein hydrogel structure acts as a geometrical cue to establish synthetic cell polarity in vitro by compressing vesicles into different shapes upon pH stimuli. This spatially well-defined microenvironment can mimic the dynamic native cell matrix, allowing us to investigate how synthetic cells react to and interact with external mechanical cues.

2. Results and Discussion

GUVs themselves can be generated either by electroformation, gentle hydration of dehydrated lipids, inverted emulsion transfer, or by microfluidic jetting. Procedures to handle these delicate objects are still not consummate.[19] They encompass sedimentation with high-density fluids, immobilization on functionalized surfaces,[20] manipulation by micropipette aspiration,[21] or microfluidic systems.[12,19] As an alternative, but still being compatible with these established protocols, our 3D BSA protein hydrogel GUVs traps were fabricated in a layer-by-layer procedure via two-photon polymerization process, using Rose bengal as the photoinitiator for BSA monomers (Scheme S1, Supporting Information). In contrast to other trapping approaches, surface functionalization for avoiding GUV-surface adhesion is not required for the 3D printed hydrogel chips. The electroformed GUVs filled with high-density solution, like sucrose, can spontaneously sink down into the hydrogel microchambers. Trapping in the chambers prevents GUVs from being flushed away and from being mechanically deformed by applied flow. To rationally design a trap that can be easily adapted to different sizes of GUVs, we chose a simple module consisting of a solid cube ($14 \times 14 \times 14$ µm) extrude-cut by half-cylinders (Diameter: 10 µm) on both sides (Figure S3a, Supporting Information). These GUV traps were then arranged into a 10×10-module array. By controlling the distance of rows and columns in the array, we can generate two different types of trap chips: individual traps, or group traps. With 1 µm distance for both rows and columns, the individual trap chip can be used to capture GUVs one by one within 81 separated cylinder wells (**Figure 2**a; and Figure S1a, Supporting

Information). The GUVs here utilized were obtained through electroformation,[22] composed of DOPC(1,2-dioleoyl-sn-glycero-3-phosphocholine) and doped with 0.5 mol% Atto655-DOPE(1,2-dioleoyl-sn-glycero-3-phosphoethanolamine) for fluorescence detection. By extending the row distance to 15 µm, groups of GUVs can be trapped between two full rows (Figure 2b; and Figure S1b, Supporting Information), in order to manipulate many vesicles at once, or to enforce their communications and interactions. The sizes of GUVs to be trapped depend on the diameters or distances, respectively (Figure 2c). GUVs with diameters larger than the gap distance are filtered out. The selective trapping of GUVs by the hydrogel chip, either as individuals or in groups, allows their size to be roughly controlled, as a first criterion toward establishing geometric anisotropy of vesicles.

In addition to allowing for a flexible size-filtering design, BSA hydrogel also shows great potential in generating smart pH stimuli-responsive microdevices that can be used to dynamically mimic the native cellular microenvironment in vitro. The isoelectric point of BSA is close to pH 5, where a protein has no net charge and fewer ion–dipole interactions. Therefore, the structures absorb less water than at higher pH and thus cover the smallest area at pH 5.[18a,23] Due to the larger number of ionized amino acids in BSA, swelling of the structures can be induced at higher pH. However, precisely controlling pH can be difficult. To improve controllability, the swelling capability can be effectively tuned by fabrication parameters, such as slicing distance (layer distance), laser power, and laser scan speed, as shown in **Figure 3**; and Figure S2 (Supporting Information). The area swelling ratios of $14 \times 14 \times 15$ µm cubes can be tuned from 1.1 to 1.7 (Figure 3b–d). A larger slicing distance results in lower crosslinking density and allows more water to enter inside the hydrogel, which in turn increases the swelling ability. Similarly, lower laser power also increases the swelling ratio to 1.7 (Figure 3c), but loses the spatial resolution of printing. Because of the lower crosslinking degree under low laser power, the structures printed at 30 mW laser power are ≈30% larger than when printed at 50 mW (Figure S2d, Supporting Information). When varying the scan speed, structures at pH between 5 and 8 have weak swelling capability and the maximal swelling ratio at pH 11 can only reach a factor of 1.5 (Figure 3d).

The controllable swelling ratios of 3D printed hydrogel structures enable a programmable templating of GUV geometries with pH-stimuli responsive GUVs traps. Due to the swelling effect of the traps, the total structure occupies a larger volume, which should in turn shrink the free inner volume of the chambers. The swelling behavior of a square-frame trap was first investigated. It was designed by extruding cut $15 \times 15 \times 15$ µm square wells in the center of $45 \times 45 \times 15$ µm cuboid (Figure 3e). The hydrogel frame can swell 1.57 ± 0.15 fold (mean ± s.d.) at pH 11 compared to pH 5; however, no shrinking of the inner area was observed. The potential reason is the increased surface tension at the inner side of the hydrogel frame, scaling inversely with radius. To improve the design toward a truly contractible and at the same time anisotropic trap, the structure was divided into eight separate small rectangular modules (Figure 3f). Allowing 2 µm distance between the modules in the relaxed state should support swelling in all directions. Because there exists no
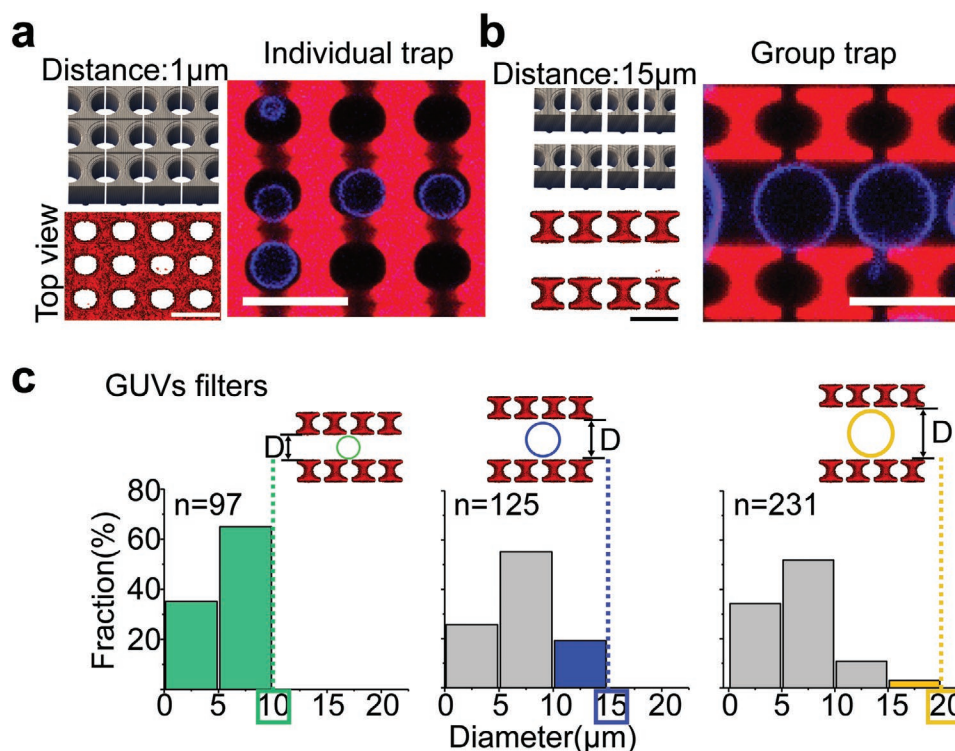
Figure 2. 3D-printed protein hydrogel chips filtering and trapping different-sized vesicles. a) Chip design for trapping individual GUVs, scale bar 20 µm. Left (top): All microchambers were integrated in one chip. Left (bottom): top view. Right: trapping individual GUVs in separated hydrogel chambers. b) Chip design for group trapping, scale bar 20 µm. Left (top): The chip was combined with separated units as barriers with certain distance. Left (bottom): top view. Right: trapping GUVs in between the hydrogel barriers. c) 3D printed hydrogel traps as GUV filters with different row distances. n: number of trapped GUV numbers. D: distance.

physical connection between the module surfaces as in the previous design, the section area of the inner free space could be decreased to 75% (±2.2%) in the swollen state when the pH was changed from 5 to 11 (Figure 3f, bottom right). Another advantage of the modular design is that the distance between the modules can be varied, in order to accommodate a larger growth regime and anisotropic compression. Small distances may lead to surface contact between the modules during swelling, which induces shape changes and restricts the overall compression effect (Figure S4, Supporting Information).

In order to evaluate the mechanical effects that can be obtained by vesicle compression, the pH stimuli-responsive hydrogel chambers were now applied to deform trapped membrane vesicles. The basic module of the group trap can swell in both x- and y- directions and thus occupies free space between modules after shifting pH from 5 to 11 (**Figure 4**a). In the rows, the distance between the modules was significantly reduced. Perpendicularly to this, two neighboring modules fused to yield a lens-shaped well, but with larger diameter than the half-cylinder at pH5. The channels between the individual barriers were also narrowed to about 50% (Figure 4a). In response to the pH stimuli, the hydrogel can process fast swelling within 1 min, supporting a dynamic mimicry of the cell microenvironment in vitro (Figure 4b; and Movie S1, Supporting Information). The trapped GUVs were now investigated by optical microscopy (Figure 4c). After shifting the pH to 11, the spherical vesicles were compressed by the closing

walls, flattening them and forcing them into nonspherical symmetry (Figure 4d,e). The distance between the two rows was 11.97 ± 0.34 µm at pH 11, so that vesicles larger than ≈12 µm in diameter were compressed. With increasing confinement under swelling conditions over a time course of 6 min, the curvature became anisotropic, with flat areas facing the hydrogel and increased curvatures in the free zone (Figure 4d). At the same time, the membrane tension was increased, due to the loss of spherical symmetry and volume conservation, which imposes some constraints on the aspect ratio σ (length vs width) of the vesicles that can be reached by this procedure without compromising membrane integrity. An aspect ratio of up to about twofold (length vs width) could, however, be easily reached by this setup (Figure S5, Supporting Information). Importantly, the hydrogel swelling is reversible, and the vesicle shapes can thus be switched between spherical and elongated by alternating between the two pH values (Figure 4e).

Furthermore, different designs of the hydrogel structures allow us to induce unusual shapes of the GUVs, and thus, membrane geometries, by varying the contact zones between the hydrogel and the vesicles. The cylindrical chip was designed by extruding a cylinder (diameter, 15 µm) in the center of a cube ($20 \times 20 \times 20$ µm) (**Figure 5**a; and Figure S3d, Supporting Information). Then the cube with the cylindrical well was quartered. This chip was used to trap vesicles of ≈15 µm diameter. When the pH was increased from 5 to 11, the four separated modules swelled centripetally and compressed the captured membrane

ADVANCED
SCIENCE NEWS
www.advancedsciencenews.com

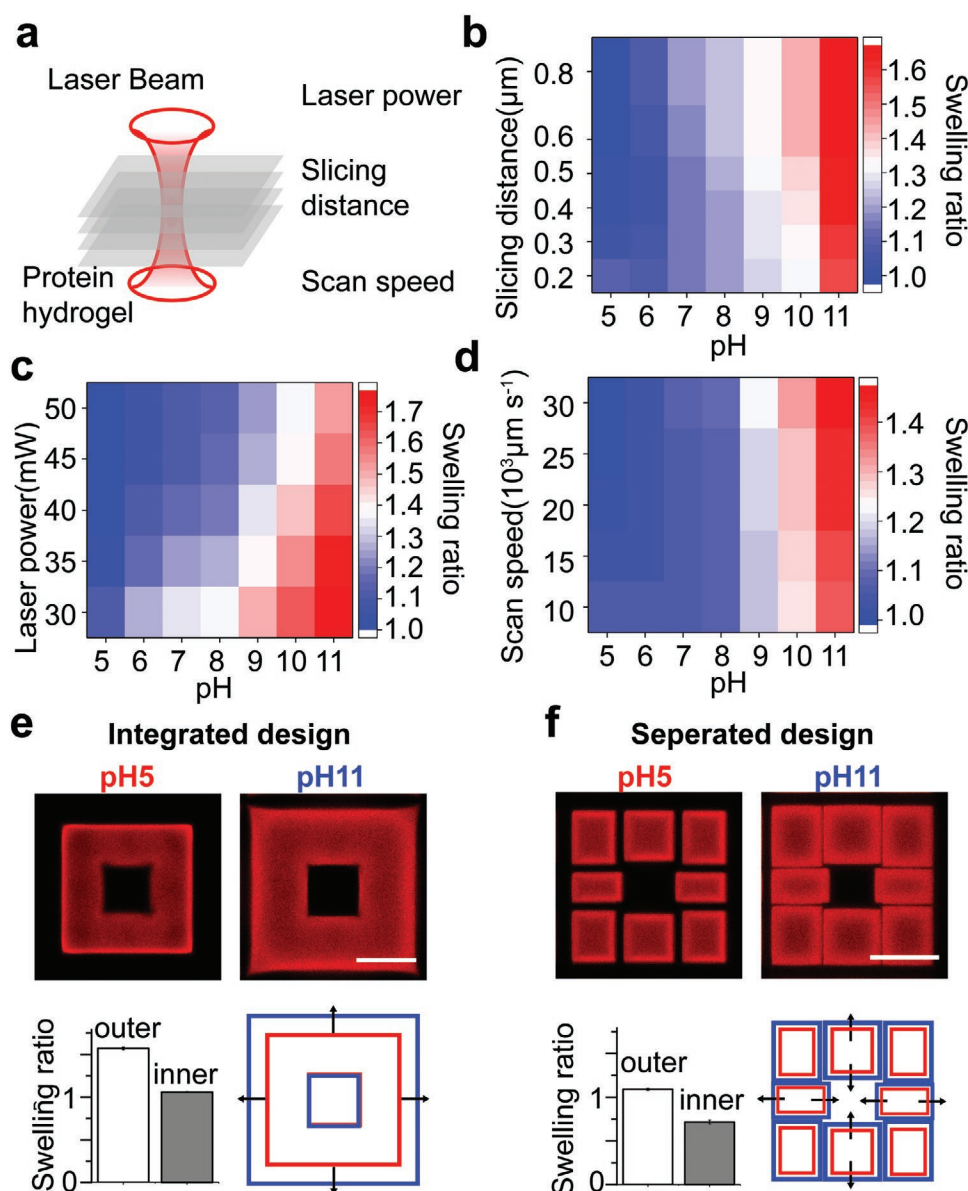NANO · MICRO
small
www.small-journal.com

Figure 3. pH-stimuli responsive protein hydrogel. a) Laser fabrication of hydrogel layer by layer with two-photon excitation. b–d) Tuning pH-stimuli swelling ratio by varying slicing distance (b), laser power (c), and laser scan speed (d). Printing parameters: b) laser power: 50 mW, Scan speed: 30 000 μm s^{-1}; c) Slicing distance: 0.5 μm, Scan speed: 30 000 μm s^{-1}; d) Slicing distance: 0.5 μm; laser power: 50 mW. e,f) pH-dependent swelling of integrated chip and the combined chip (Slicing distance: 0.5 μm; laser power: 50 mW; Scan speed: 30 000 μm s^{-1}), scale bar 20 μm. Top: confocal imaging of the swelling effect under different pH. Bottom (left): swelling ratios of outer and inner area. Bottom (right): directional swelling. Area swelling ratio is defined as A/A_0, where A_0 is the area of the structure at pH 5, printed under slicing distance: 0.5 μm, laser power: 50 mW, scan speed: 30 000 μm s^{-1}.

vesicle. The area of the cross-section was reduced, in turn the height was increased. Similarly, with alternative designs, GUVs can be deformed to other shapes like cross prisms, cubes, and triangular prisms (Figure 5b,c). Due to the surface tension of membrane vesicles, the templated cross-prismatic, cubic, and triangular prismatic vesicles all formed curved corners and spherical domes.

Having shown that GUVs can not only be reversibly compressed, but also molded into arbitrary nonspherical shapes by our laser-printed BSA pH-responsive hydrogel structures, we next aim to demonstrate how these mechanical constraints may

influence membrane structure and dynamics in the shaped vesicles. In particular, GUVs have long been used to elucidate the molecular details of lipid phase separation; however, their usually spherical symmetry and isotropic structure have significantly limited the comparability of these model membranes with biological ones. In physiological environments, cells acquire and maintain spatial and functional asymmetry of their plasma membrane[24] in response to external mechanical cues. Similarly, in model membrane systems exhibiting visible lipid domains enriched in cholesterol and saturated lipids, strong correlations between membrane composition and 3D
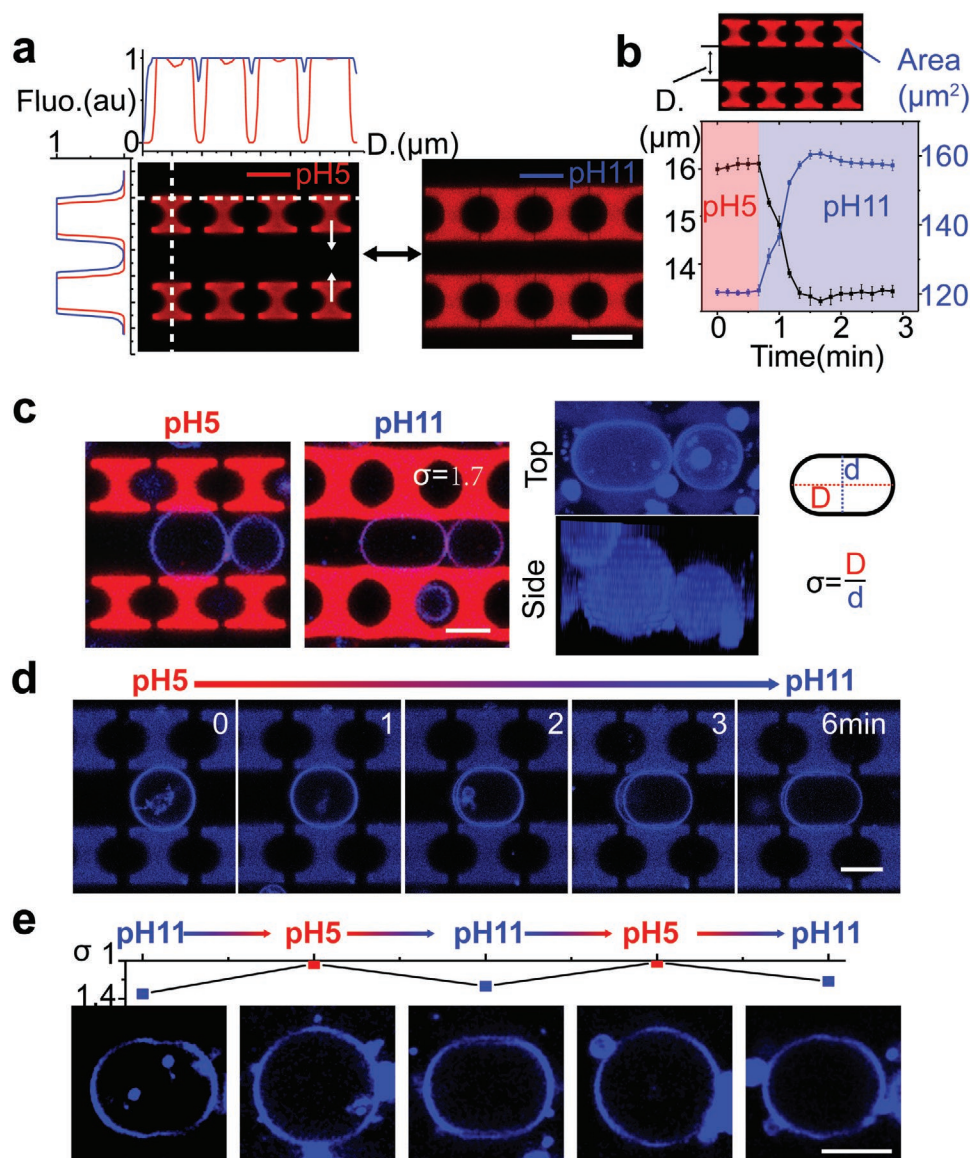
Figure 4. Reversibly deforming membrane vesicles by pH. a) Swelling effect of group trap at increased pH, scale bar 20 µm. The line plots demonstrate the swelling in both x- and y-axis, respectively. b) Response of geometry factors area and distance when transitioning to pH 11 solution. c) Swelling chip deforming DOPC GUV, scale bar 10 µm. Right: top and side view of deformed GUVs. d) Dynamic deformation of GUV by exchanging pH from 5 to 11, scale bar 10 µm. e) Reversibility of GUV aspect ratio (σ) by alternating pH, scale bar 10 µm.

vesicle shape could be observed, which suggest that, in turn, mechanical constraints will lead to significant membrane transformations.[24,25]

The phase-separated GUVs we investigated in our stimuli-responsive hydrogel cages consisted of ternary lipid mixtures composed of cholesterol (Ch), sphingomyelin (SM), and the unsaturated phospholipid DOPC, with a molar ratio of 2:2:1 at room temperature.[26] The mixture can separate into two coexisting membrane phases: a liquid-ordered phase (L_o) enriched in SM and Ch; and a liquid-disordered (L_d) phase consisting primarily of DOPC. To discriminate between the L_o and L_d phases by fluorescence microscopy, we used 0.3%NBD-DSPE and 0.2% Atto655-DOPE, respectively. The spherical phase-separated GUVs were trapped in the triangular prismatic hydrogel

chips (Figure S3c, Supporting Information). When the GUVs were compressed by the swelling hydrogel chamber under pH stimuli, the vesicles deformed to fit the diminished inner area, often accompanied by a large-scale reorganization and fusion of the domains on their membrane surface (Figure S6, Supporting Information). In several cases, particularly for vesicles with large domains, the spherical vesicle was transiently deformed upon compression into a dumbbell geometry, due to line tension between L_o–L_d domains,[27] acquiring a clear curved neck at the domain boundary. Typically, the dumbbell-shaped phase-separated vesicle then rotated within the contracted hydrogel cavity, in order to adapt the space change and relax back into a spherical (yet compacted) energetically favorable shape (**Figure 6**b; and Figure S7, Movie S2 for top view of 3D
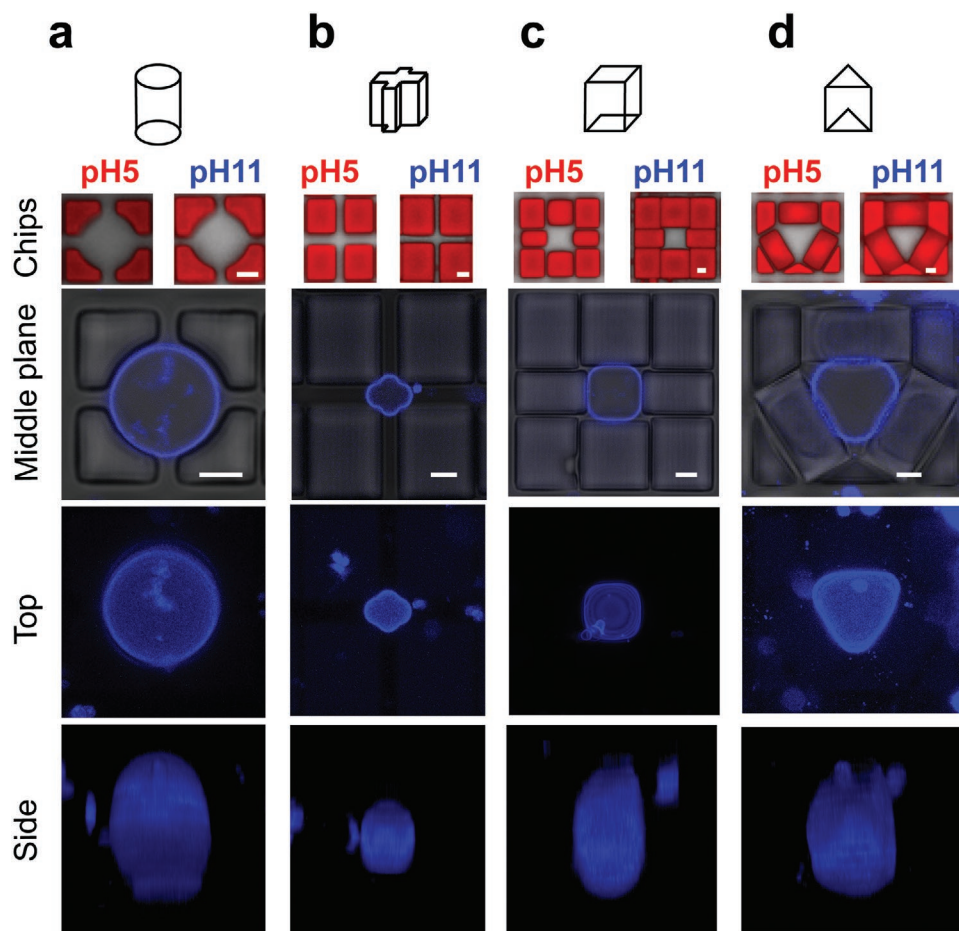
Figure 5. Various 3D hydrogel designs for templating DOPC vesicles into different shapes: a) cylinder, b) cross prism, c) cube, d) triangular prism. The schemes in the first row show the 3D geometries of trap wells. Below the schemes are the top views of the chips in response to different pH, scale bar 5 µm. Third row from top: confocal imaging of the middle cross-section of vesicles, scale bar 5 µm. The bottom two rows represent the 3D z-stack reconstitution of different geometrical vesicles.

imaging, and Movie S3 for orthogonal view, Supporting Information). Occasionally, however, the compression led to the fission of a Lo domain away from the trapped GUV membrane (i.e., budding as a way to overcome line tension,[28] ultimately changing the overall membrane composition of the remaining "mother" vesicle (Figure 6c; and Movie S4, Supporting Information). In the control experiment without the swelling traps, no triggered deformation events were detected upon pH change from 5 to 11 (Figure S8, Supporting Information). Thus, the ability to exert gentle but significant mechanical pressure on GUVs in our custom-designed protein hydrogel cages opens up a new way of manipulating vesicle model systems, inducing features that could be of great relevance in the design of cellular mimicries, such as shape and differential membrane curvature, respectively, tension.

The surface geometry that determines membrane dynamics also affects the spatiotemporal patterns and oscillations formed by reaction-diffusion systems.[29] A striking example of a reaction-diffusion system is the Min protein system, consisting of the proteins MinC, MinD, and MinE, which oscillate between the cell poles and spatially position the bacterial cell division machinery in *Escherichia coli*.[30] In vitro reconstitution of the

Min system on micropatterned surfaces or in microcompartments has shown that the geometry of the boundaries plays a pivotal role in its pattern formation and pace-making.[10,31] Recently, the Min system has been encapsulated into 3D spherical compartments, motivated by the long-term goal of creating a self-reproducible synthetic cell.[32] Unlike in vivo, this reconstituted reaction-diffusion system reveals several distinct oscillation modes, namely pulsing oscillations, pole-to-pole oscillations, and circling and trigger waves.[32b] Causes for such diverse behaviors are differences in protein concentration, vesicle size, proteins ratio, or the isotropic geometry. Here, we used the 3D hydrogel shaped vesicles to demonstrate how the anisotropy of microenvironment influences the reaction-diffusion system.

We encapsulated the oscillating Min system (MinD (50% EGFP-MinD) & MinE) in negatively charged GUVs (DOPC:DOPG(1,2-dielaidoyl-sn-glycero-3-phospho-(1'-rac-glycerol); molar ratio, 4:1) with an inverted emulsion method (cDICE method[33]). Subsequently, the vesicles were trapped within the hydrogel chips. Similar to what has been reported before,[32b] the majority of the uncompressed vesicles was showing pulsing oscillations, for which all proteins simultaneously oscillate
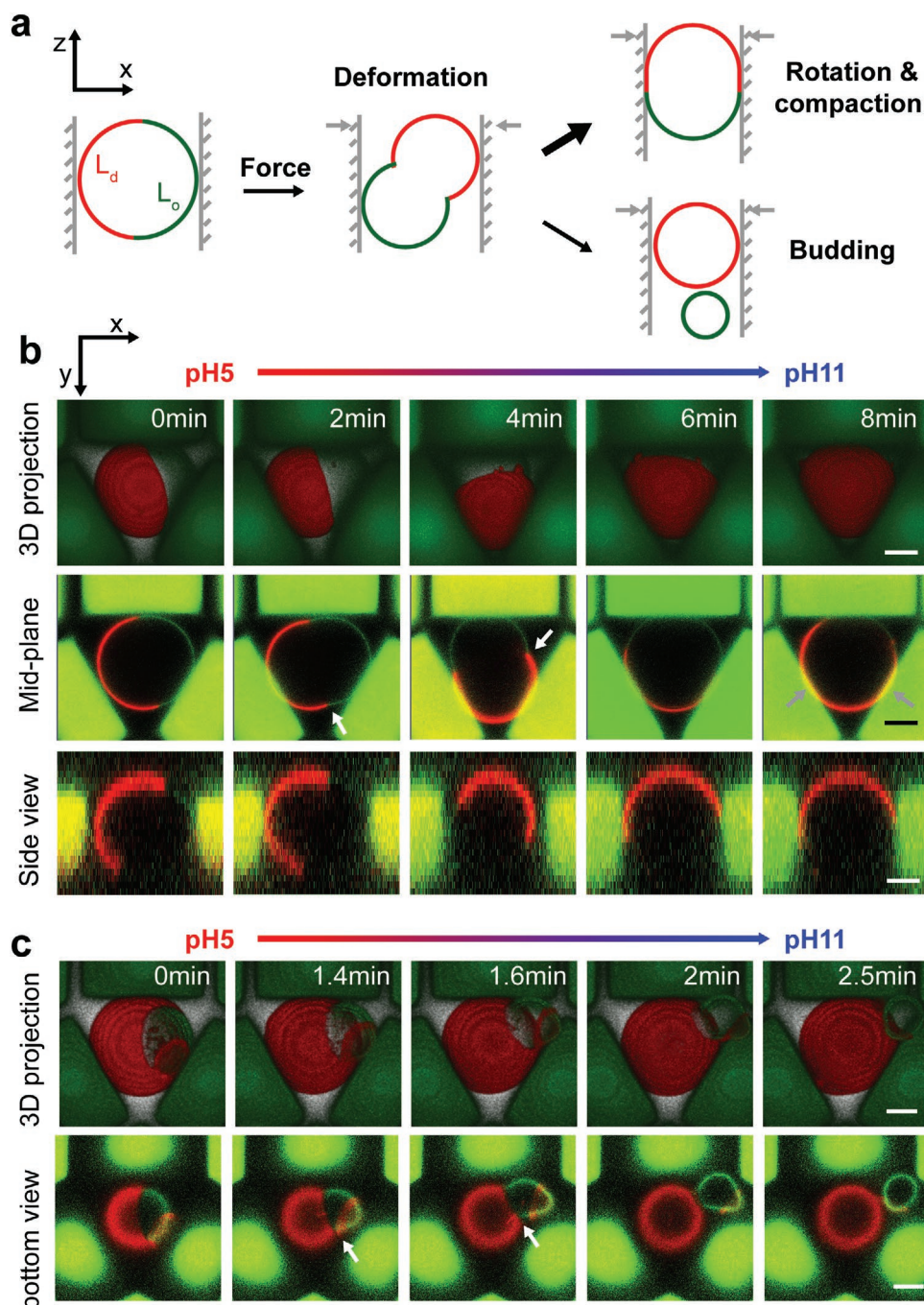
Figure 6. a) Scheme of dynamic lipid phase reorganization adapting to the space-induced membrane deformation. b) Dynamic membrane domain reorganization under pH-induced compression in the hydrogel chambers, scale bar 5 µm. c) Membrane budding driven by the compression of the hydrogel chambers, scale bar 5 µm. GUVs were produced from DOPC:SM:cholesterol (2:2:1) and labeled with NBD-DSPE (green) and Atto655-DOPE (red). The 3D projections of 3D images were compiled from Z-stack confocal images with ZEN software.

between the vesicle lumen and the inner membrane leaflet (**Figure 7**a). After the pH change from 5 to 11, vesicles that did not get deformed by the hydrogel structures, approximately maintained the oscillation frequency (Figure [7b,c]). Since the electrical gradient across the vesicle membrane restricts proton transfer to the inside, intact vesicles showed minor and slow changes of the pH in the vesicle lumen.[34] This minor change

can be buffered away by the chosen buffer system. However, for vesicles that were compressed due to the hydrogel swelling, we observed an increase in oscillation frequency compared to their uncompressed state (Figure 7d–f; and Movie S5, Supporting Information). We suspect a correlation to the resulting change in aspect ratio of the vesicles (Figure S9, Supporting Information). Larger aspect ratios result in shorter diffusion paths from
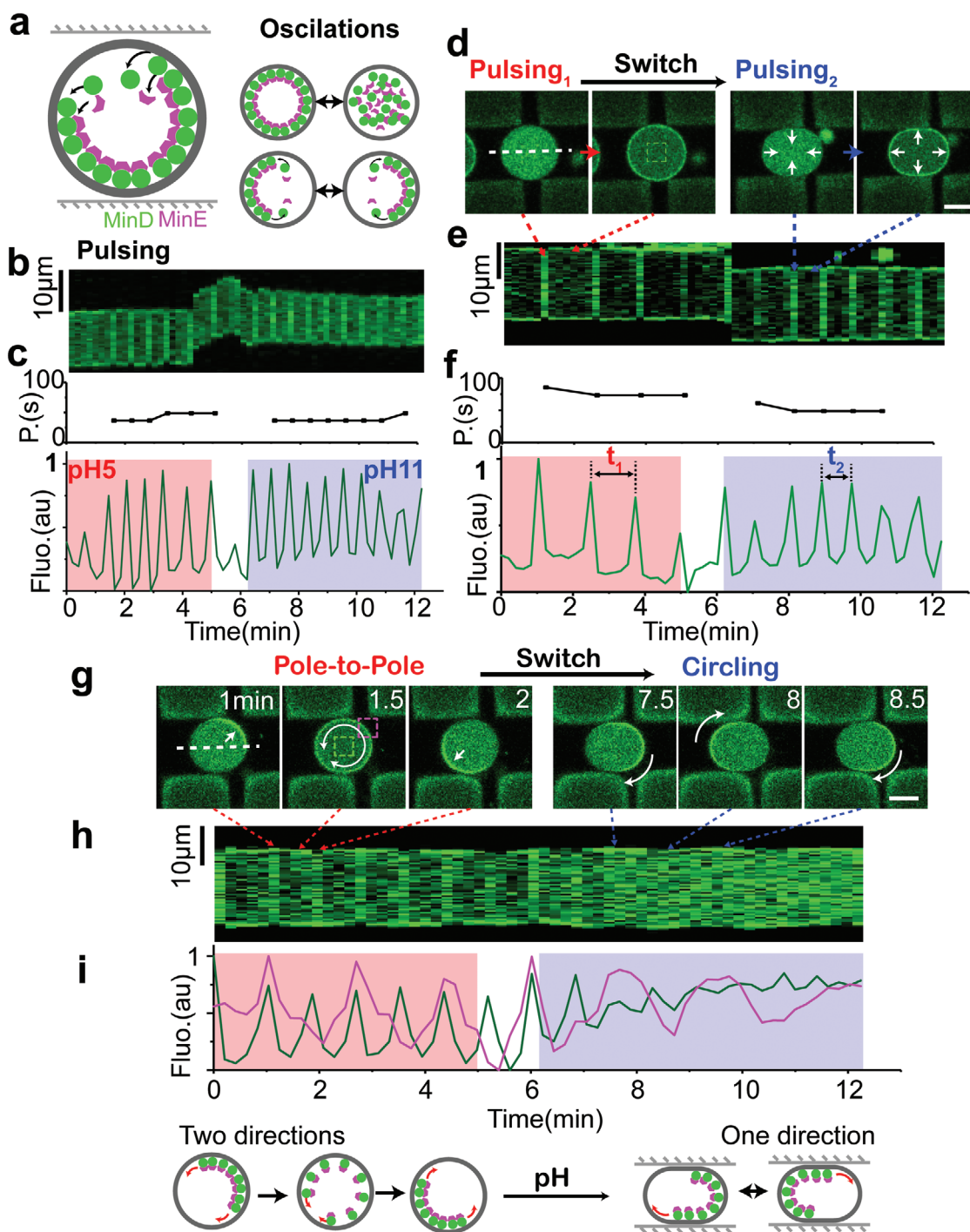
1906259 (7 of 10)

Figure 7. Protein oscillation modes transition in response to change in vesicle geometry. a) Schematic of Min protein oscillations in vesicles. b,c) Pulsing oscillation in a spherical vesicle under different pH conditions. d–f) Pulsing oscillation acceleration during vesicles compression. g–i) Min oscillation modes transition from pole-to-pole to circling. (d), (g), and (j) show imaging frames from the confocal time series of oscillation (1.5×10^{-6} M MinD, 1.5×10^{-6} M eGFP-MinD, 3×10^{-6} M MinE, 5×10^{-3} M ATP). Scale bar: 10 μm. (b), (e), and (h) demonstrate the kymograph of the oscillation. The white dash lines on the vesicles indicate the position for the kymograph analysis. (c) and (f) (top) show the periods change inside vesicles. (c), (f) (bottom), and (i) either describe the fluorescence oscillation inside vesicles (green) or on the membrane (purple). The green and purple dash box shows the position for measuring the oscillation curves.

vesicle lumen to vesicle membrane and could explain a shorter period of oscillation. On the other hand, membrane vesicle compression leads to changes in membrane tension, which

could also affect the affinity of Min proteins to lipid bilayer and, consequently, alter the reaction diffusion rates. Indeed, in vitro reconstitution revealed that a reduced membrane affinity

of Min proteins results in faster traveling waves.[35] As tense membranes resist the deformation, compressed vesicles would display an increasing membrane tension when compared to uncompressed spherical vesicles. Many studies have shown that protein–membrane interactions are strongly inhibited at high membrane tension.[36] Thus, to evaluate this hypothesis, only MinD was encapsulated inside GUVs. Indeed, the compression of vesicles with the swelling hydrogel reduced the overall binding of MinD to the membranes (Figure S10a, Supporting Information). This result could be corroborated, as similar findings were observed in trapped vesicles under increased membrane tension undergoing a hypotonic shock (Figure S10b, Supporting Information).

Intriguingly, besides the changes in oscillation frequency, in some cases we observed that the oscillation mode transitioned into a different mode in response to the change in geometry. Figure 7g–i; and Movie S6 (Supporting Information) show a vesicle that initially exhibited pole-to-pole oscillations, in which the maximum protein concentration alternates between the two opposing membrane poles of the vesicle. Upon hydrogel swelling and thus vesicle compression, the protein oscillation switched to a different mode, which was previously described as circling waves:[32,36b] the protein still is only bound to a small region on the membrane at a time, but now continuously revolves, i.e., "circles," on the inside surface of the vesicle. Thus, we showed that dynamically regulating the anisotropy of spherical vesicles with pH-stimuli 3D hydrogel chip provides us with new mechanical cues for the investigation of reaction-diffusion systems in 3D artificial microenvironments.

3. Conclusion

We have developed a new toolbox for mechanical manipulation of GUVs—model membrane vesicles that constitute the basis for the engineering of advanced protocells and that should ideally be subject to defined shape transformations. This is particularly desirable when reconstituting membrane polarity- or shape-dependent protein systems, such as bacterial cell division machineries that request explicitly nonspherical geometries.[10] Our hydrogel devices are based on custom-printed BSA protein that can be switched by pH, and are thus fully biocompatible. Their dimensions are limited only by the optical resolution of the two-photon laser used for printing. We demonstrated that the swelling ratio depends on the laser power used for printing, such that even more complex designs with differential volume expansion could in principle be realized. This opens up a fully new way of using GUVs as custom-made platforms to probe the functionality of reconstituted cellular modules in bottom-up synthetic biology. Our technique thus opens up exciting potential applications for synthetic cell and tissue engineering.

Supporting Information

Supporting Information is available from the Wiley Online Library or from the author.

Conflict of Interest

The authors declare no conflict of interest.

[1] H. Jia, P. Schwille, *Curr. Opin. Biotechnol.* **2019**, *60*, 179.

[2] H. Jia, M. Heymann, F. Bernhard, P. Schwille, L. Kai, *New Biotechnol.* **2017**, *39*, 199.

[3] C. Xu, S. Hu, X. Chen, *Mater. Today* **2016**, *19*, 516.

[4] K. Göpfrich, I. Platzman, J. P. Spatz, *Trends Biotechnol.* **2018**, *36*, 938.

[5] R. Dimova, M. Carlos *The Giant Vesicle Book*, CRC Press, Boca Raton, FL **2019**.

[6] E. Sezgin, I. Levental, S. Mayor, C. Eggeling, *Nat. Rev. Mol. Cell Biol.* **2017**, *18*, 361.

[7] S. K. Vogel, F. Greiss, A. Khmelinskaia, P. Schwille, *eLife* **2017**, *6*, e24350.

[8] M. Dezi, A. Di Cicco, P. Bassereau, D. Lévy, *Proc. Natl. Acad. Sci. USA* **2013**, *110*, 7276.

[9] C. Yeaman, K. K. Grindstaff, W. J. Nelson, *Physiol. Rev.* **1999**, *79*, 73.

[10] K. Zieske, P. Schwille, *eLife* **2014**, *3*, e03949.

[11] a) A. Yamada, S. Lee, P. Bassereau, C. N. Baroud, *Soft Matter* **2014**, *10*, 5878; b) F. Fanalista, A. Birnie, R. Maan, F. Burla, K. Charles, G. Pawlik, S. Deshpande, G. H. Koenderink, M. Dogterom, C. Dekker, *ACS Nano* **2019**, *13*, 5439; c) T. Robinson, P. S. Dittrich, *ChemBioChem* **2019**, *20*, 1701.

[12] J. Korlach, C. Reichle, T. Müller, T. Schnelle, W. Webb, *Biophys. J.* **2005**, *89*, 554.

[13] M. Théry, V. Racine, M. Piel, A. Pépin, A. Dimitrov, Y. Chen, J.-B. Sibarita, M. Bornens, *Proc. Natl. Acad. Sci. USA* **2006**, *103*, 19771.

[14] Y. T. Kim, S. Bohjanen, N. Bhattacharjee, A. Folch, *Lab Chip* **2019**, *19*, 3086.

[15] M. Bao, J. Xie, A. Piruska, W. T. Huck, *Nat. Commun.* **2017**, *8*, 1962.

[16] B. Kaehr, J. B. Shear, *Proc. Natl. Acad. Sci. USA* **2008**, *105*, 8850.

[17] P.-S. Li, I.-L. Lee, W.-L. Yu, J.-S. Sun, W.-N. Jane, H.-H. Shen, *Sci. Rep.* **2014**, *4*, 5600.

[18] a) M. R. Lee, I. Y. Phang, Y. Cui, Y. H. Lee, X. Y. Ling, *Small* **2015**, *11*, 740; b) C. L. Lay, M. R. Lee, H. K. Lee, I. Y. Phang, X. Y. Ling, *ACS Nano* **2015**, *9*, 9708.

[19] T. Robinson, P. Kuhn, K. Eyer, P. S. Dittrich, *Biomicrofluidics* **2013**, *7*, 044105.

[20] D. Stamou, C. Duschl, E. Delamarche, H. Vogel, *Angew. Chem.* **2003**, *115*, 5738.

1906259 (9 of 10)

[21] B. Sorre, A. Callan-Jones, J.-B. Manneville, P. Nassoy, J.-F. Joanny, J. Prost, B. Goud, P. Bassereau, *Proc. Natl. Acad. Sci. USA* **2009**, *106*, 5622.

[22] A. Khmelinskaia, H. G. Franquelim, E. P. Petrov, P. Schwille, *J. Phys. D: Appl. Phys.* **2016**, *49*, 194001.

[23] T. Peters Jr., *All About Albumin: Biochemistry, Genetics, and Medical Applications*, Academic Press, San Diego, CA **1995**.

[24] D. Hoekstra, O. Maier, J. M. van der Wouden, T. A. Slimane, S. C. van IJzendoorn, *J. Lipid Res.* **2003**, *44*, 869.

[25] K. Bacia, P. Schwille, T. Kurzchalia, *Proc. Natl. Acad. Sci. USA* **2005**, *102*, 3272.

[26] S. L. Veatch, S. L. Keller, *Biophys. J.* **2003**, *85*, 3074.

[27] A. J. García-Sáez, S. Chiantia, P. Schwille, *J. Biol. Chem.* **2007**, *282*, 33537.

[28] F. Jülicher, R. Lipowsky, *Phys. Rev. Lett.* **1993**, *70*, 2964.

[29] a) E. Frey, J. Halatek, S. Kretschmer, P. Schwille, *Physics of Biological Membranes*, Springer, Cham, Switzerland **2018**, p. 229;

b) D. Thalmeier, J. Halatek, E. Frey, *Proc. Natl. Acad. Sci. USA* **2016**, *113*, 548.

[30] M. Loose, E. Fischer-Friedrich, J. Ries, K. Kruse, P. Schwille, *Science* **2008**, *320*, 789.

[31] a) J. Schweizer, M. Loose, M. Bonny, K. Kruse, I. Mönch, P. Schwille, *Proc. Natl. Acad. Sci. USA* **2012**, *109*, 15283; b) K. Zieske, P. Schwille, *Angew. Chem., Int. Ed.* **2013**, *52*, 459.

[32] a) K. Zieske, G. Chwastek, P. Schwille, *Angew. Chem., Int. Ed.* **2016**, *55*, 13455; b) T. Litschel, B. Ramm, R. Maas, M. Heymann, P. Schwille, *Angew. Chem., Int. Ed.* **2018**, *57*, 16286.

[33] M. Abkarian, E. Loiseau, G. Massiera, *Soft Matter* **2011**, *7*, 4610.

[34] M. Megens, C. E. Korman, C. M. Ajo-Franklin, D. A. Horsley, *Biochim. Biophys. Acta* **2014**, *1838*, 2420.

[35] B. Ramm, T. Heermann, P. Schwille, *Cell. Mol. Life Sci.* **2019**, *76*, 4245.

[36] a) M. Saleem, S. Morlot, A. Hohendahl, J. Manzi, M. Lenz, A. Roux, *Nat. Commun.* **2015**, *6*, 6249; b) M. Simunovic, G. A. Voth, *Nat. Commun.* **2015**, *6*, 7219.

1906259 (10 of 10)